JOURNAL OF MATERIALS SCIENCE 25 (1990) 4047–4053

High-speed sliding indentation of ceramics: thermal effects

T. N. FARRIS, S. CHANDRASEKAR*
*School of Aeronautics and Astronautics, and *School of Industrial Engineering, Purdue University, West Lafayette, Indiana 47907, USA*

A diamond indentor is attached to the periphery of an aluminium wheel and slid against ferrite and sapphire surfaces at high speed. A high-frequency response infrared sensor is used to measure the average diamond tip temperature and a piezoelectric dynamometer is used to measure the normal and tangential forces acting on the indentor. The analytical procedure estimates the heat flux at the contact as the product of the shear traction and the tangential velocity. The heat flux is used in conjunction with a Green's function to calculate the interface temperature and the tangential surface stress. The calculated and measured grain tip temperatures are compared and the relative magnitudes of the mechanical and thermal surface stresses are calculated. Finally, the importance of thermal effects on the wear and surface finishing of ceramics is discussed.

1. Introduction

The sliding indentation process is of intrinsic interest to materials processing and tribology. It closely approximates the nature of asperity contacts between sliding surfaces and occurs in several applications including materials processing operations such as grinding and machining, bearings, electrical contacts, piston to cylinder contacts in engines, and magnetic head to media interfaces in computer storage systems. In many of these sliding contacts at least one or both of the members are made of ceramics. Ceramics show particular promise in high-speed sliding applications due to their stability, high hardness, and strength at elevated temperatures. This paper presents a portion of a research programme directed at characterizing thermal effects at high-speed sliding ceramic interfaces. These thermal effects can be broadly classified into three categories.

1. The high temperatures generated in the surface/subsurface of the members as a consequence of frictional heating.
2. Thermal stresses in the contacting solids, both transient and residual, induced by the frictional heating process.
3. The corresponding wear and failure modes.

In addition, mechanically induced stresses due to normal and tangential tractions at the sliding contacts are present.

The high temperatures and stresses generated in turn play an important role in influencing the very friction and wear processes out of which they arise. They significantly alter the mechanical, magnetic, and electrical properties of the contacting surfaces [1–6]. For instance, in some zirconium oxide ceramics, the temperatures and stresses generated can cause an improvement in the fracture toughness of the ceramic. Thermally induced stresses are particularly important in dictating crack nucleation and propagation and plastic deformation processes in ceramics [7], thereby controlling the wear and fracture resistance of the component. A scanning electron micrograph of a typical stress-induced crack on a ground ceramic surface is shown in Fig. 1. It is therefore critical that these effects be well understood and quantified so that the tribological performance of these ceramics and the property changes occurring in them can be predicted and controlled.

There have been several studies pertaining to the analysis and measurement of interface temperatures in sliding contact [8–15]. Foremost amongst these are the classical papers of Blok [8], Jaeger [9], and Archard [10]. In recent years, with the development of high-frequency response infrared sensors, radiation measurement techniques have emerged as a powerful tool for estimating sliding contact temperatures [12–15]. However, microindentation contacts, which have been studied extensively under static loading conditions, have been neglected in most of the high-speed sliding temperature studies. Reliable temperature measurements, in addition to providing insight into various physical and chemical processes that can occur at sliding interfaces, will enable the analysis of thermal stresses developed at these contacts.

In this paper we present results of an investigation into the temperatures and stresses generated in high-speed ceramic-to-ceramic sliding contacts. Interface temperatures are measured for the case of a diamond indentor sliding against polycrystalline Ni–Zn ferrite and single-crystal sapphire specimens. Calculations of the average interface temperature are compared with experimentally measured values. In addition, the mechanical and thermal stresses developed in ferrite are calculated utilizing the experimental measurements of the forces and the calculated interface temperatures.

0022–2461/90 $03.00 + .12

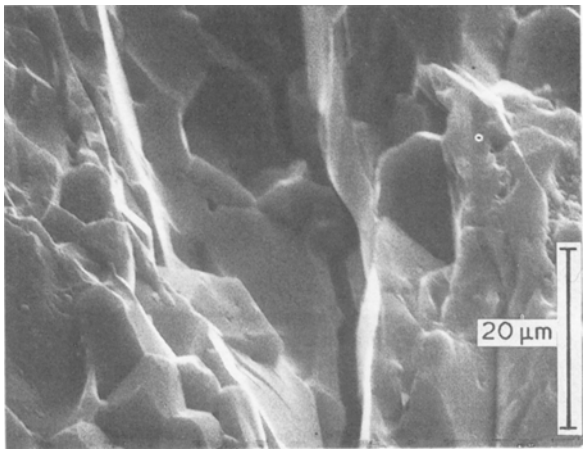

Figure 1 Scanning electron micrograph of a typical crack found on a ground ceramic surface.

2. Experiments

2.1. Configuration

Table I gives the relevant mechanical and thermal properties of Ni–Zn ferrite, sapphire, and diamond, the materials used in this study. Sapphire is anisotropic and the average properties given in the literature [16, 17] are reproduced in Table I.

Fig. 2 depicts schematically the experimental arrangement used in the temperature measurement studies. The diamond indentor, a single abrasive grain, is mounted on the periphery of the aluminium disc. In one experimental configuration, shown in Fig. 2, the infrared sensor monitors the radiation from the diamond cutting point just after it makes an indentation and passes over the hole (approximately 2 mm diameter) in the ferrite or sapphire workpiece. Because sapphire is transparent (> 90% transmittance) in the infrared wavelength window (1 to 5 μm) [16], the infrared radiation at the diamond–sapphire interface can be monitored without making a hole in the sapphire sample. Therefore, for comparison purposes, an additional experimental configuration is used in which the diamond tip is observed, using the infrared sensor, through a 1 mm thick sapphire sample.

2.2. Calibration

The multiple-element infrared sensor used in the experimental study consists of four individual indium antimonide (InSb) cells (Santa Barbara Research Corporation) and a high-speed thermal monitor (Vanzetti Systems Corporation). The cells are mounted on a Dewar flask cooled with liquid nitrogen to 77 K. InSb responds to radiation in the 0.65 to 5.3 μm range which is appropriate for the present experiments. It

TABLE I Material properties

Property	Ferrite	Diamond	Sapphire
E (GPa)	191	1000	390
ν	0.2	0.2	0.23
K (W m^{-1} °C^{-1})	8	1000	27
c (J g^{-1} °C^{-1})	0.81	0.525	0.75
ρ (g cm^{-3})	5.3	3.5	3.98

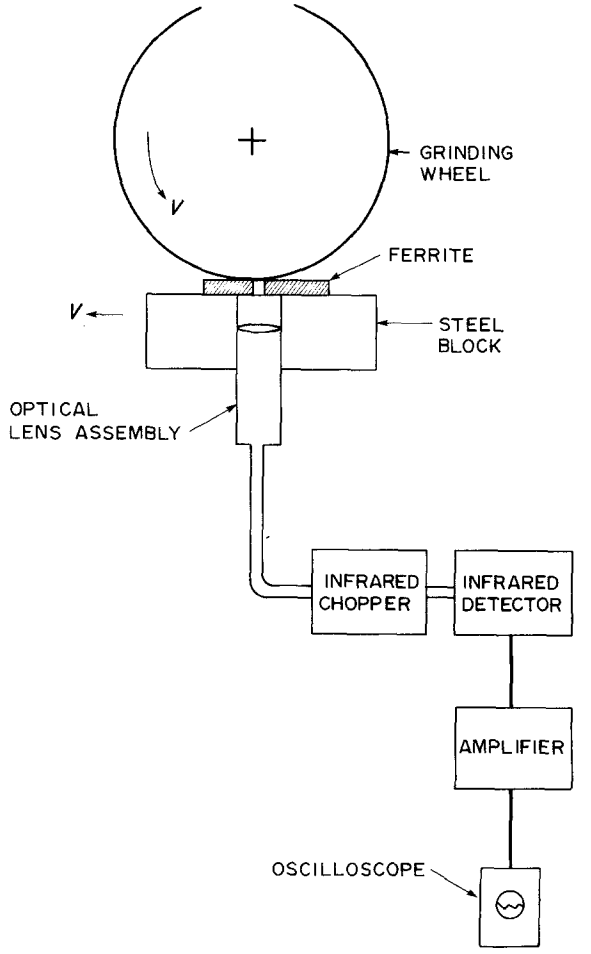

Figure 2 Schematic illustration of the experimental arrangement used for temperature measurements.

can be conveniently used in the photovoltaic mode to give response times as low as 1 μsec. When cooled with liquid nitrogen, the performance of InSb improves by an order of magnitude due to longer wavelength sensitivity and decreased thermal noise [18]. The detector elements are coupled to fibre-optic lens assemblies which transmit the radiation from the source to the detector plane. With the use of the multiple element sensor, temperature measurements could be made simultaneously at five locations. The smallest spot size achievable in the present arrangement is 40 μm. The output of each detector element is amplified and recorded in a multi-channel digital storage oscilloscope. In the present study, because temperature measurements are made at only one point, only one of the InSb detector elements was used.

2.2.1. Time constant determination

The detector was calibrated both statically and dynamically. Static calibration was performed by exposing it to a standard infrared source. Dynamic calibration was performed in two different ways.

1. A camera shutter is placed between a calibrated infrared source and the detector. The shutter opening is controlled to expose the source for periods as short as 100 m sec.

2. The detector was exposed to the calibrated infrared source through a hole near the periphery of a

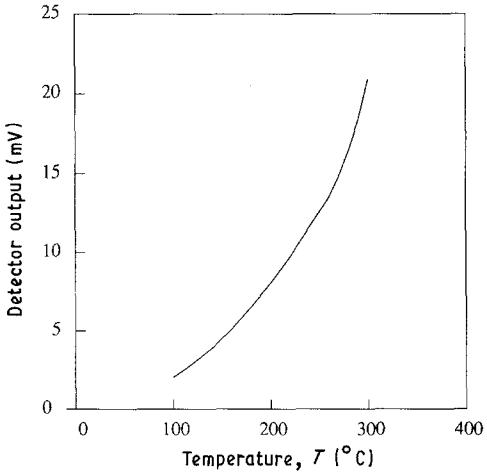

Figure 3 Calibration curve for the infrared detector for a 40 μm spot size.

spinning aluminium disc. This scheme utilizes a situation (temperature pulse) that is almost identical to that of the high-speed sliding indentation experiment.

The time constants of the detector elements were determined as the time taken for the response to reach 63% of the final value for a step temperature input. Each detector element was calibrated separately and the responses of the four InSb elements are almost identical with the output increasing faster at higher temperatures. A sample of this output in the 100 to 400° C temperature range is shown in Fig. 3. The time constants of these InSb cells were 6.8 μsec. The Vanzetti high-speed detector had a time constant of 7.4 μsec. This response time is adequate for measurement of the average diamond grain tip temperature.

2.2.2. Emissivity

Emissivity measurements were made on the diamond tip, the Ni–Zn ferrite, and the sapphire samples used in the study. The diamond tip emissivities were measured both before and after rubbing against the ferrite and sapphire to see if there were any changes. This was done because the diamond tip that is observed during the grinding experiments has repeatedly come into contact with the Ni–Zn ferrite and sapphire. However, there was no detectable change in the emissivity before and after rubbing. The specimen was heated to known temperatures in the range 50 to 680° C and infrared radiation emitted by the specimen was compared with radiation emitted by a blackbody source in the same range. From these measurements the effective emissivity of the specimen could be determined. For details of the emissivity measurements using a spectral emissometer, see [18].

The effective emissivity of the diamond tip was found to be 0.19 and that of ferrite to be 0.81 at 680° C. The emissivity change with temperature was marginal at temperatures over 500° C. When the diamond tip was heated to 680° C for 1 h the emissivity fluctuated by about 0.02 from the above value. In all of the experimental measurements the above emissivity values were used. Corrections were also made for the radiation acceptance angle of the multiple element sensor. The emissivity corrections were directly incorporated in the sensor circuit electronics. However, the emissivity of sapphire is small [16] and no corrections for it need to be included. These corrections are discussed in detail in [18].

2.3. Temperature results

Table II gives the measured diamond tip temperatures when indenting Ni–Zn ferrite and sapphire at three different sliding velocities. The measurements were made by observing the diamond tip through a hole in the ceramic workpiece. These results show that the average diamond tip temperature during the sliding indentation of sapphire is ~900 to 1300° C, which is higher than the tip temperature during contact with Ni–Zn ferrite (~600 to 700° C). The average tip temperature increases with increasing sliding velocity between the diamond tip and the ceramic surfaces.

In a second set of experiments, the infrared sensor was mounted with its optical lens assembly beneath a 1 mm thick sapphire specimen whose *c*-axis was perpendicular to the surface. The top surface of the sapphire specimen was indented with the diamond tip and the infrared radiation emitted from the interface during the sliding contact was measured using the infrared sensor; the infrared radiation having been transmitted through a 1 mm thickness of the sapphire specimen. The temperature measurements were conducted when the indentor crossed the axis of the fibre-optic lens assembly.

In order to obtain a true temperature measurement, it is necessary to correct for the infrared transmission losses through the sapphire specimen and for the radiation generated within the sapphire due to the sapphire specimen being heated to a high temperature. The infrared transmittance of the sapphire was estimated from reference experiments as 0.95 at a temperature of 680° C. The corrections for the transmittance are given in [18]. No corrections were made for the emittance of sapphire which is small [16]; due to neglecting this the maximum error for a surface temperature of 1000° C is estimated to be no greater than 25° C [18]. Corrections were also not made for scattering of the radiation at the diamond–sapphire interface during the indentation process. However, spot size corrections were made for transmission of the radiation through the sapphire sample [18].

Table III gives the measured diamond indentor temperatures during sliding contact with sapphire. The temperatures were obtained during sliding contacts under nominally identical contact conditions.

The mean value of the measured interface temperature is 1225° C compared to a mean value of 1060° C for the diamond tip when observed through a hole in the sapphire under identical sliding conditions. This

TABLE II Average diamond temperatures

Wheel velocity, V (m sec^{-1})	Temperature (° C)	
	Against ferrite	Against sapphire
25	570 ± 30	920 ± 65
32	620 ± 35	1060 ± 45
37	690 ± 30	1270 ± 80

Sliding conditions: depth of cut 0.01 mm; table velocity 23.4 mm sec^{-1}; average diamond tip diameter 15 μm.

suggests that the temperatures of the diamond tip when measured through a hole in the workpiece are not the true interface temperature. However, in view of the difficulty in observing the interface (especially in materials not transparent in the infrared) during the indentation process, the studies on sapphire (with and without a hole) demonstrate that the measurement through the hole is a good approximation of the interface temperature. The observed scatter in the temperatures in Table III is probably due to scattering of the infrared radiation that could take place at the diamond–sapphire interface and in slight differences in the nature of each contact.

Graphitization of diamond has sometimes been known to occur at temperatures as low as 1200° C [19]; this temperature has been exceeded in the present study during the sliding indentation of sapphire by diamond.

2.4. Force measurements

The normal and tangential forces exerted on the diamond tip during the sliding indentation of ferrite were measured by mounting the ferrite workpiece on a three-component piezoelectric force sensor (Kistler). The measured forces and the friction coefficient are listed in Table IV. These forces are used in the heat flux calculations.

3. Analysis

The analysis utilizes the thermoelastic Green's functions for the moving heat source found by Barber [20] and Bryant [21]. A line source of heat of strength, Q, per unit length per unit time moves with velocity, V, to the right along the surface of an elastic half-space (Fig. 4). The surface temperature is found as

$$T(x', 0) = \frac{Q}{\pi K} e^{-\beta x'/2} K_0\left(\frac{\beta}{2} x'\right) \quad (1)$$

where K is the thermal conductivity, $\beta = V/\kappa$, $\kappa = K/\rho c$ is the thermal diffusivity, ρ is the density, c is the specific heat, $x' = x - Vt$ where t is time, and K_0 and K_1 are the modified Bessel functions of the second kind [22]. This result was also given by Jaeger [9] (see Carslaw and Jaeger [23], Section 10.7). Barber [20] calculated the surface displacements and the tangential stress at the surface due to this temperature distribution, while Bryant [21] later obtained the subsurface stresses and displacements. The tangential stress at the surface is found as

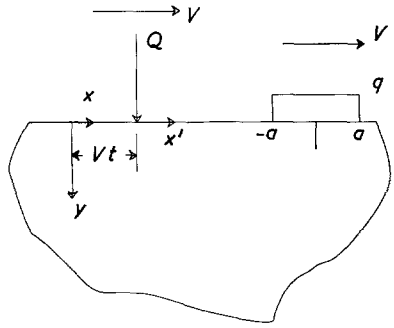

Figure 4 Point and distributed heat sources.

$$\sigma_{xx}(x', 0) = \frac{2E\alpha Q}{\pi(1-\nu)\beta K}\left[-\frac{1}{x'} + \frac{\beta}{2} K_1\left(\frac{\beta}{2} x'\right) e^{-\beta x'/2}\right] \quad (2)$$

where E is Young's modulus, α is the thermal expansion coefficient, ν is Poisson's ratio, and plane strain is assumed. Note that we interpret $K_0(-x) = K_0(x)$ and $K_1(-x) = -K_1(x)$. The remaining in-plane stresses, σ_{yy} and τ_{xy}, are zero at the surface. The tangential stress is bounded at the surface and the heat source does not induce any singular stresses.

Equations 1 and 2 can be used as Green's functions to calculate the surface temperature and tangential stress due to a distributed heat source. This is accomplished by writing $Q = q(\xi)\mathrm{d}\xi$ and $x' = x' - \xi$ in Equations 1 and 2 where $q(\xi)$ is the strength of the distributed source. These equations are then integrated with respect to ξ. If q is uniform from $\xi = -a$ to $\xi = a$, the integrals can be evaluated in closed form and are given in the Appendix.

The frictional energy dissipated per unit time during sliding can be calculated as

$$W = \mu N V \quad (3)$$

where μ is the coefficient of friction and N is the normal force applied to the grain. For a circular grain contact of radius a, the heat generated per unit area of contact per unit time is

$$q = \frac{\mu N V}{\pi a^2} \quad (4)$$

Most of the heat generated is conducted into the diamond grain while the remainder is conducted into the ferrite workpiece. Ramanath and Shaw [24] have shown that for large Peclet number

$$L = \frac{2Va}{\kappa} > 20 \quad (5)$$

TABLE III Average diamond temperatures for six measurements

Contact number	Diamond indentor temperature (° C)
1	1140
2	1280
3	1170
4	1210
5	1250
6	1300
Mean temperature	1225

Sliding conditions: sliding against sapphire; depth of cut 0.01 mm; table velocity 23.4 mm sec^{-1}; average diamond tip diameter 15 μm; wheel velocity 32 m sec^{-1}.

TABLE IV Measured forces

Wheel velocity	37 m sec^{-1}
Work velocity	23.4 mm sec^{-1}
Depth of cut	0.01 mm
Normal force	0.71 N
Tangential force	0.18 N
Coefficient of friction	0.25

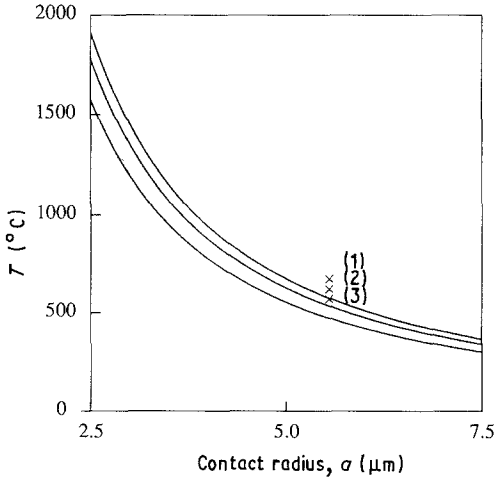

Figure 5 Average diamond tip temperature for ferrite, $N = 0.71$ N and $\mu = 0.25$. (——) Analytical results, (△) experimental results; (1) $V = 37\,\mathrm{m\,sec^{-1}}$, (2) $V = 32\,\mathrm{m\,sec^{-1}}$, (3) $V = 25\,\mathrm{m\,sec^{-1}}$.

the percentage of heat conducted into the ferrite is

$$R = \frac{1}{1 + \left[\dfrac{(K\rho c)_D}{(K\rho c)_F}\right]^{1/2}} \approx 0.12 \qquad (6)$$

where the subscripts F and D refer to ferrite and diamond, respectively.

Replacing q in Equation A3 with Rq from Equations 6 and 4 allows the surface temperature distribution caused by a grain tip of length $2a$ to be calculated. The two-dimensional analysis assumes that the heat flux distribution is uniform in the direction perpendicular to sliding. The three-dimensional heat flux distribution is approximated by using the average heat generated per unit area in the two-dimensional model. The surface temperature distribution is integrated numerically to yield an average diamond tip temperature. The average diamond tip temperature is shown in Fig. 5 as a function of contact radius and sliding velocity for the forces given in Table IV.

Comparison of calculated and measured temperatures requires the contact size. Assuming Hertz contact by a diamond spherical indentor of radius 7.5 μm loaded by $N = 0.71$ N, one can calculate a maximum contact pressure of 41 GPa which is well above the Vickers hardness of ferrite, $H = 7.35$ GPa. Therefore, the contact area is approximated as the normal load over the hardness. Assuming circular contact, the contact radius is calculated to be

$$a = \left(\frac{1}{\pi} N/H\right)^{1/2} \approx 5.55\,\mu\mathrm{m} \qquad (7)$$

The Peclet number for this radius is $L = 150$ for $V = 25\,\mathrm{m\,sec^{-1}}$ and the heat partitioning model (Equation 6) is valid. The measured temperatures are shown in Fig. 5 assuming $a = 5.55\,\mu$m. The agreement between the measured and calculated temperatures is better than expected, even though the temperature analysis is two-dimensional.

Next the mechanical and thermal surface stresses are calculated. The thermal stress model assumes elastic deformation and, for comparison, mechanical stresses relevant to elastic deformation are also plotted.

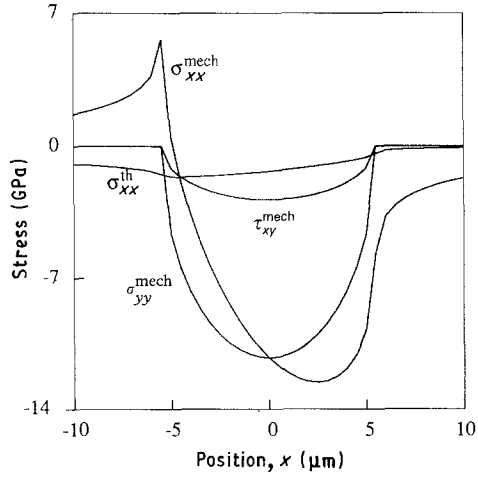

Figure 6 Comparison of mechanical and thermal surface stresses for ferrite, $V = 37\,\mathrm{m\,sec^{-1}}$, $N = 0.71$ N, $\mu = 0.25$, and $a = 5.5\,\mu$m.

The mechanical stress calculation assumes a sliding Hertz line contact of length $2a$ and maximum pressure $p_0 = 3/2H$ giving a total load of 0.71 N. The mechanical stresses are taken from Johnson [25] as

$$\sigma_{yy}(x', y) = -p_0[1 - (x'/a)^2]^{1/2} \qquad |x| < a \qquad (8)$$

$$\tau_{xy}(x', y) = \mu\sigma_{yy} \qquad |x| < a \qquad (9)$$

$$\sigma_{xx}(x', y) = -2\mu p_0 x'/a + \sigma_{yy}(x', y) \qquad |x| < a \qquad (10)$$

$$\sigma_{xx}(x', y) = -2\mu p_0(x'/a \pm [(x'/a)^2 - 1)]^{1/2} \qquad |x| > a \qquad (11)$$

The mechanical and thermal surface stresses are plotted in Fig. 6. The thermal stress is generally small relative to the mechanical stress. The thermal tangential stress reduces the tensile sliding tangential stress behind the contact while it enhances the compressive stress ahead of the contact.

4. Discussion

4.1. Temperatures

The average surface temperature generated by a single diamond indentor during sliding contact with polycrystalline Ni–Zn ferrite and single-crystal sapphire has been measured using a multiple element infrared sensor. Jaeger's analysis has been used to calculate the surface temperature generated by a diamond indentor in contact with Ni–Zn ferrite. For a normal load of 0.71 N and a sliding velocity of $37\,\mathrm{m\,sec^{-1}}$ the temperature rise is measured as 690° C and calculated as 575° C. The agreement between the model and the experiment is quite good considering the fact that a two-dimensional analysis is used to model a three-dimensional experiment. A similar calculation was not performed for single-crystal sapphire because of its anisotropy.

The interface temperature is generally found to increase with increasing sliding velocity between the indentor and the ceramic; the temperatures being in the range 550 to 700° C for the diamond–ferrite contact and in the range of 900 to 1300° C for diamond–sapphire contact, see Table II. Direct observations of the infrared radiation from the diamond–sapphire interface were also made by using the infrared detector to monitor this radiation through the infrared-

transparent sapphire crystal. These revealed the temperatures of the diamond tip in the contact zone to be about 200 to 250° C greater than the temperature of the diamond tip immediately after contact (as observed through a hole in the sapphire specimen). A reason for the difference may lie in the decay of the diamond tip temperature in the short period after contact due to the high thermal conductivity of diamond. The results, however, demonstrate that temperature measurements of the diamond tip made by observing it through a hole in the ceramic are a reasonably good estimate of the actual contact temperature, especially in view of the difficulty in observing the interface in most indentation contact configurations.

The interface temperature of 550 to 700° C measured in diamond–ferrite contacts is close to the Curie temperature of Ni–Zn ferrite (this is typically between 300 and 600° C). Therefore, localized changes in the magnetic properties of the ferrite could occur during contact.

4.2. Thermal stresses

Because the model is reasonably successful at predicting the surface temperature, it is used to make preliminary calculations of thermal stresses which can be compared to mechanical stresses. The comparison of mechanical and thermal stresses is called preliminary as it assumes that all stresses are elastic.

The tangential thermal surface stress is compressive. It reduces the tensile mechanical stress behind the contact while it increases the mechanical stress ahead of the contact. The tensile tangential stress is important to the crack driving force for indentation-induced cracks which break the surface (Fig. 1). The thermal stress appears to reduce the live crack-driving force. However, abrasive machining processes such as grinding usually lead to compressive residual tangential stresses which are beneficial as they suppress the growth of the surface-breaking crack in bending tests performed subsequent to grinding [26]. The live tensile tangential stress would tend to cause compressive residual stresses so the compressive thermal stress may reduce the beneficial compressive residual stress.

4.3. Implications

The temperatures generated at high-speed indentation contacts induce significant thermal stresses, both transient and residual. This contribution is important and needs to be considered along with the stresses induced by purely mechanical loading while analysing high-speed microindentation contacts. The temperature studies show that localized heating above the Curie temperature of ferrites, with associated undesirable changes in their magnetic properties, can occur during the abrasive machining of ferrites. Graphitization of diamond is sometimes known to occur at a temperature as low as 1200° C and this temperature is attained in some of the diamond–sapphire contacts. This would contribute to the wear of the indentor, again the implications for the abrasive machining of ceramics are obvious.

Future analytical work will include making subsurface stress calculations. These may shed light on the initiation of grinding and polishing cracks and the residual stress distribution caused by grinding. Additional effort will be directed at making calculations for anisotropic materials such as sapphire and for a quarter plane to help assess the effect of the hole, through which the infrared radiation is transmitted, on the temperature. Experimental work will centre on further temperature measurements and estimating the live stresses induced by the sliding indentor.

Acknowledgements

This work was partially supported by the National Science Foundation (NSF) through grants MSM 8706920 (Tribology Programme, Dr J. Larsen-Basse, Programme Monitor) and MSM 8706919A (Programme in Materials Engineering and Processing, Dr R. Komanduri, Programme Monitor). We would like to thank D. Jacobs, Purdue Physics Department, for help with the emissivity measurements. We are also grateful to Professor M. C. Shaw, Arizona State University, for loan of the Vanzetti thermal monitor.

Appendix

Equation 1 is integrated to give the surface temperature distribution for a uniform heat source of length $2a$ and strength q as

$$T = \frac{2q}{\pi K\beta} I_1 \qquad \text{(A1)}$$

where

$$\begin{aligned} I_1 = {} & -(X-A)e^{-(X-A)}\{K_0[-(X-A)] \\ & + K_1[-(X-A)]\} \\ & + (X+A)e^{-(X+A)}\{K_0[-(X+A)] \\ & + K_1[-(X+A)]\} \qquad X < -A \end{aligned} \qquad \text{(A2)}$$

$$\begin{aligned} I_1 = {} & (X+A)e^{-(X+A)}\{K_0(X+A) - K_1(X+A)\} \\ & - (X-A)e^{-(X-A)}\{K_0[-(X-A)] \\ & + K_1[-(X-A)]\} \qquad -A < X < A \end{aligned} \qquad \text{(A3)}$$

$$\begin{aligned} I_1 = {} & (X+A)e^{-(X+A)}\{K_0(X+A) - K_1(X+A)\} \\ & - (X-A)e^{-(X+A)}\{K_0(X-A) \\ & - K_1(X-A)\} \qquad X > A \end{aligned} \qquad \text{(A4)}$$

where $X = Vx'/2\kappa$ and $A = Va/2\kappa$.

The analogous tangential surface stress is

$$\sigma_{xx}(x', 0) = \frac{2E\alpha q}{\pi(1-\nu)K\beta}(-I_2 + I_3) \qquad \text{(A5)}$$

where

$$I_2 = \ln(|X-A|/|X+A|) \qquad \text{(A6)}$$

$$\begin{aligned} I_3 = {} & -e^{-(X-A)}K_0[-(X-A)] \\ & + e^{-(X+A)}K_0[-(X+A)] \\ & - (X-A)e^{-(X-A)}\{K_0[-(X-A)] \\ & + K_1[-(X-A)]\} \\ & + (X+A)e^{-(X+A)}\{K_0[-(X+A)] \\ & - K_1[-(X+A)]\} \qquad X < -A \end{aligned} \qquad \text{(A7)}$$

$$I_3 = -e^{-(X+A)}K_0(X+A) + e^{-(X-A)}K_0[-(X-A)] + (X-A)e^{-(X-A)}\{K_0[-(X-A)] + K_1[-(X-A)]\} - (X+A)e^{-(X+A)}\{K_0(X+A) - K_1(X+A)\} \quad -A < X < A \quad \text{(A8)}$$

$$I_3 = e^{-(X-A)}K_0(X-A) - e^{-(X+A)}K_0(X+A) + (X-A)e^{-(X-A)}\{K_0(X-A) - K_1(X-A)\} - (X+A)e^{-(X+A)}\{K_0(X+A) - K_1(X+A)\} \quad X > A \quad \text{(A9)}$$

References

1. R. J. STOKES, in "The Science of Ceramic Machining and Surface Finishing", Vol. I, edited by B. J. Hockey and S. J. Schneider (National Bureau of Standards, Washington, 1972) p. 343.
2. D. JOHNSON-WALLS, A. G. EVANS, D. B. MARSHALL and M. R. JAMES, *J. Amer. Ceram. Soc.* **69** (1986) 44.
3. E. KLOCKHOLM and J. WOLFE, "Dead Layers in Mn–Zn and Ni–Zn Ferrites", Research Report (IBM T. J. Watson Research Center, New York, 1983).
4. S. CHANDRASEKAR, M. C. SHAW and B. BHUSHAN, in "Tribology and Mechanics of Magnetic Storage Systems", Vol. III, ASLE Special Publication 21, edited by B. Bhushan, D. Bogy and N. Eiss (American Society for Lubrication Engineering, Chicago 1986) p. 41.
5. B. LAWN and T. R. WILSHAW, "Fracture of Brittle Solids" (Cambridge University Press, 1976).
6. B. LAWN and T. R. WILSHAW, *J. Mater. Sci.* **10** (1975) 1049.
7. D. RIGNEY, (ed.) "Fundamentals of Friction and Wear of Materials", ASM Materials Science Seminar, October 1980 (American Society for Metals, Metals Park, Ohio, 1981).
8. H. BLOK, *Proc. Inst. Mech. Eng.* **2** (1937) 222.
9. J. C. JAEGER, *Proc. Royal Soc. New South Wales* **56** (1942) 203.
10. J. F. ARCHARD, *Wear* **2** (1958) 438.
11. B. BHUSHAN and N. H. COOK, *J. Lub. Tech.* **95** (1973) 535.
12. J. E. MAYER and M. C. SHAW, *ASLE J.* **13** (1956) 21.
13. R. GULINO, S. BAIR, W. O. WINER and B. BHUSHAN, *J. Tribol.* **108** (1986) 29.
14. S. CHANDRASEKAR, T. N. FARRIS and B. BHUSHAN, *ibid.* (1990) in press.
15. T. UEDA, A. HOSOKAWA and A. YAMAMOTO, *J. Engng Ind.* **107** (1985) 127.
16. "Optical Properties and Applications of Linde-Cz Sapphire", Union Carbide, Technical Bulletin F-CPD 72950 (1972).
17. "Engineering Properties of Ceramics", Battelle Memorial Institute, Technical Report AFML-DR 66-52, June 1966.
18. S. CHANDRASEKAR and T. N. FARRIS, "Infrared Grinding Temperatures", Technical Report, Schools of Industrial Engineering and Aeronautics and Astronautics, Purdue University, March 1989.
19. R. M. CHRENKO and H. M. STRONG, "Physical Properties of Diamond", Technical Report No. 75CRD089, General Electric Company, October 1975.
20. J. R. BARBER, *J. Appl. Mech.* **51** (1984) 636.
21. M. D. BRYANT, *ibid.* **55** (1988) 87.
22. M. ABRAMOWITZ and I. A. STEGUN, "Handbook of Mathematical Functions", 9th Edn (Dover, 1972) Ch. 9.
23. H. S. CARSLAW and J. C. JAEGER, "Conduction of Heat in Solids", 2nd Edn (Oxford University Press, 1959).
24. S. RAMANATH and M. C. SHAW, *J. Engng Ind.* **110** (1988) 15.
25. K. L. JOHNSON, "Contact Mechanics" (Cambridge University Press, 1985) Ch. 2, 7.
26. R. SAMUEL, S. CHANDRASEKAR, T. N. FARRIS and R. H. LICHT, *J. Amer. Ceram. Soc.* **72** (1989) 1960.

Received 18 April
and accepted 29 September 1989